Biosensors and Bioelectronics 71 (2015) 129–136

Contents lists available at ScienceDirect

Biosensors and Bioelectronics

journal homepage: www.elsevier.com/locate/bios

Dual aptamer-functionalized silica nanoparticles for the highly sensitive detection of breast cancer

Hunho Jo, Jin Her, Changill Ban *

[a] Department of Chemistry, Pohang University of Science and Technology, 77, Cheongam-Ro, Nam-Gu, Pohang, Gyeongbuk 790-784, South Korea

ARTICLE INFO

Article history:
Received 20 January 2015
Received in revised form
26 March 2015
Accepted 12 April 2015
Available online 13 April 2015

Keywords:
Silica nanoparticle
Dye-doped particle
Breast cancer
Aptamer
Biosensor
Fluorescence

ABSTRACT

In this study, we synthesized dual aptamer-modified silica nanoparticles that simultaneously target two types of breast cancer cells: the mucin 1 (MUC1)(+) and human epidermal growth factor receptor 2 (HER2)(+) cell lines. Dual aptamer system enables a broad diagnosis for breast cancer in comparison with the single aptamer system. The dye-doped silica nanoparticles offer great stability with respect to photobleaching and enable the accurate quantification of breast cancer cells. The morphological and spectroscopic characteristics of the designed Dual-SiNPs were demonstrated via diverse methods such as DLS, zeta potential measurements, UV–vis spectroscopy, and fluorescence spectroscopy. Negatively charged Dual-SiNPs with a homogeneous size distribution showed robust and strong fluorescence. In addition, Dual-SiNPs did not affect cell viability, implying that this probe might be readily available for use in an *in vivo* system. Through ratio optimization of the MUC1 and HER2 aptamers, the binding capacities of the Dual-SiNPs to both cell lines were maximized. Based on Dual-SiNPs, a highly sensitive quantification of breast cancer cells was performed, resulting in a detection limit of 1 cell/100 μL, which is significantly lower compared with those reported in other studies. Moreover, the developed detection platform displayed high selectivity for only the MUC1(+) and HER2(+) cell lines. It is expected that this valuable diagnostic probe will be a noteworthy platform for the diagnosis and prognosis of breast cancer.

1. Introduction

Circulating tumor cells (CTCs) in peripheral blood are detached epithelial cells having identical or similar carcinoma characteristics to those of the primary cancer (Gupta and Massague 2006; Pukazhendhi and Gluck 2014). They have received considerable attention as valuable biomarkers for the diagnosis and prognosis of specific tumor metastasis because the detection of CTCs is a less invasive and more reliable method than currently existing conventional methods such as radiographic photography, serum tumor marker-based detection, and biopsy (Alama et al., 2014; Mostert et al., 2009). In particular, CTCs are designated as a real-time "liquid biopsy" because of their accessibility to samples from peripheral blood (Chang et al., 2014; Nadal et al., 2013). Two main strategies are currently used for the detection of CTCs, *i.e.*, immunological assays based on monoclonal antibodies and polymerase chain reaction (PCR)-based molecular assays (Pantel et al., 2008). However, such methods exhibit various problems such as being time-consuming, costly, providing false-positive or false-negative results, and requiring large instrumentation (Gazzaniga et al., 2013; Wang et al., 2014). Therefore, a relatively rapid, inexpensive, and precise detection technique for CTCs is in high demand with respect to the early diagnosis of carcinoma metastasis.

Breast cancer is one of the most common malignant tumors and the second leading cause of cancer deaths in women (Siegel et al., 2013). According to the US National Cancer Institute Surveillance, Epidemiology, and End Results database, the averaged incidence rate of breast cancer is 123.8 cases/100,000 women/year (Johnson et al., 2013). More than 90% the cancer-related deaths are due to metastatic growth (Siegel et al., 2013). Therefore, the detection and monitoring of the metastasis of the carcinoma is most important. While several biomarkers, conventional radiologic evaluation, and histological detection cannot offer sufficient information related to tumor metastasis, CTCs certainly indicate the presence and metastatic stage of the cancer (Pantel and Alix-Panabieres, 2010). It has been known that a comparatively large number of CTCs are found in the peripheral blood of patients with breast cancer (Bidard et al., 2013). Thus, the detection of CTCs in the blood is a promising method for the early diagnosis and determination of a prognosis for breast cancer patients.

To evaluate these CTCs, various biomarkers such as the epithelial cell adhesion molecule, cytokeratin-8 (CK-8), CK-18, CK-19,

* Corresponding author. Fax: +82 54 279 5840.
E-mail addresses: jhhsst@postech.ac.kr (H. Jo), jinh0902@postech.ac.kr (J. Her), ciban@postech.ac.kr (C. Ban).

http://dx.doi.org/10.1016/j.bios.2015.04.030
0956-5663/

and hMAM have been utilized (Bertolini et al., 2006; Zhao et al., 2013). In particular, human epidermal growth factor receptor 2 (HER2) has been targeted for the detection of breast cancer CTCs since Slamon et al. (1987) discovered that the HER2 protein was over-expressed in breast cancer patients. Although numerous investigations for the detection of breast cancer cells based on HER2 have been conducted, they are limited to only HER2(+) cell lines (Gupta et al., 2011; Lu et al., 2010; Zhu et al., 2013). Because HER2 is over-expressed in only 15–20% of breast cancer patients, it cannot play a role as a confident biomarker for all types of breast cancer. Among the surface biomarkers for breast cancer, mucin-1 (MUC1) has been identified as an effective biomarkers, and it is abnormally over-expressed in greater than 90% of human breast carcinomas (Rakha et al., 2005; Singh and Bandyopadhyay, 2007). Multi-target methods using MUC1 and HER2 probes make the accurate and precise detection of CTCs in breast cancer possible.

Diverse studies on diagnosing breast cancer based on nanomaterials have been actively conducted because nanomaterials have numerous advantages over the existing detection tools such as their easy surface modification, good biocompatibility, and unique spectroscopic properties (Howes et al., 2014; Jeon et al., 2013; Lee et al., 2014; Singh et al., 2015). Of the effective nanomaterials, dye-doped silica nanoparticles (SiNPs) have been considered to be one of the best substances to be used for detection. Whereas some organic dyes have several limitations, including severe photobleaching, being costly and requiring time-consuming preparation, dye-doped SiNPs provide a high photostability, low-cost synthesis, great fluorescent signal, and good biocompatibility (Li et al., 2014; Wang et al., 2013). In particular, it has been verified that tris(2,2′-bipyridyl) dichlororuthenium(II) hexahydrate ($Ru(BPY)_3$)-doped SiNPs (Dye-SiNPs) can prevent photobleaching because the positively charged $Ru(BPY)_3$ molecule is strongly confined to the negatively charged silica matrix via a coulombic interaction, which disturbs the access of potential quenching materials from the surrounding environment (Cai et al., 2013; Herr et al., 2006; Liu et al., 2014; Smith et al., 2007). Hence, the diagnosis of breast cancer using $Ru(BPY)_3$-doped SiNPs is a most robust and valuable method.

As shown in Fig. 1, we designed a dual aptamer (MUC1 and HER2)-modified SiNP (Dual-SiNP) for the detection of breast cancer cells. This is the first time that both types of biomarkers for breast cancer have been targeted utilizing aptamers, which enables a wide-ranging diagnosis of breast cancer. First, a series of surface modifications was conducted on the core silica particles (Fig. 1A), and then their morphological and spectroscopic characteristics were analyzed through various techniques, such as transmission electron microscopy (TEM), dynamic light scattering (DLS), zeta potential measurement, ultraviolet–visible (UV–vis) spectroscopy, and fluorescence spectroscopy. The actual detection was performed in the following two steps: magnetic bead-based separation and incubation with Dual-SiNPs (Fig. 1B). The low cytotoxicity, high sensitivity, and selectivity of the developed detection system were verified through a methylthiazol tetrazolium (MTT) assay and fluorescence measurements. This newly developed diagnostic system could be a good platform for the diagnosis and prognosis of the metastasis of breast cancer.

2. Materials and methods

2.1. Functionalization of PEG-SiNPs with the dual aptamers

Prior to the immobilization of the dual aptamers on the SiNPs, the surfaces of the PEG-coated SiNPs (PEG-SiNPs) were modified by avidin. The cyanogen bromide activation method was introduced to attach avidin to the particles (March et al. 1974). Three milligrams of PEG-SiNPs were incubated under gentle stirring in 3 mL of a 2 M sodium carbonate solution for 15 min at room temperature (RT). Thereafter, 3 mL of cyanogen bromide (CNBr) in acetonitrile (0.8 g/mL) was added to the reaction solution. The mixture was stirred for an extra 15 min at RT, and then the activated particles were gathered by centrifugation, which was followed by washing with chilled distilled water twice as well as with chilled phosphate buffered saline (PBS, pH 7.4) twice. Furthermore, the resulting particles were incubated with an excess amount of avidin (100 μL of 1 mg/mL avidin in PBS) under stirring

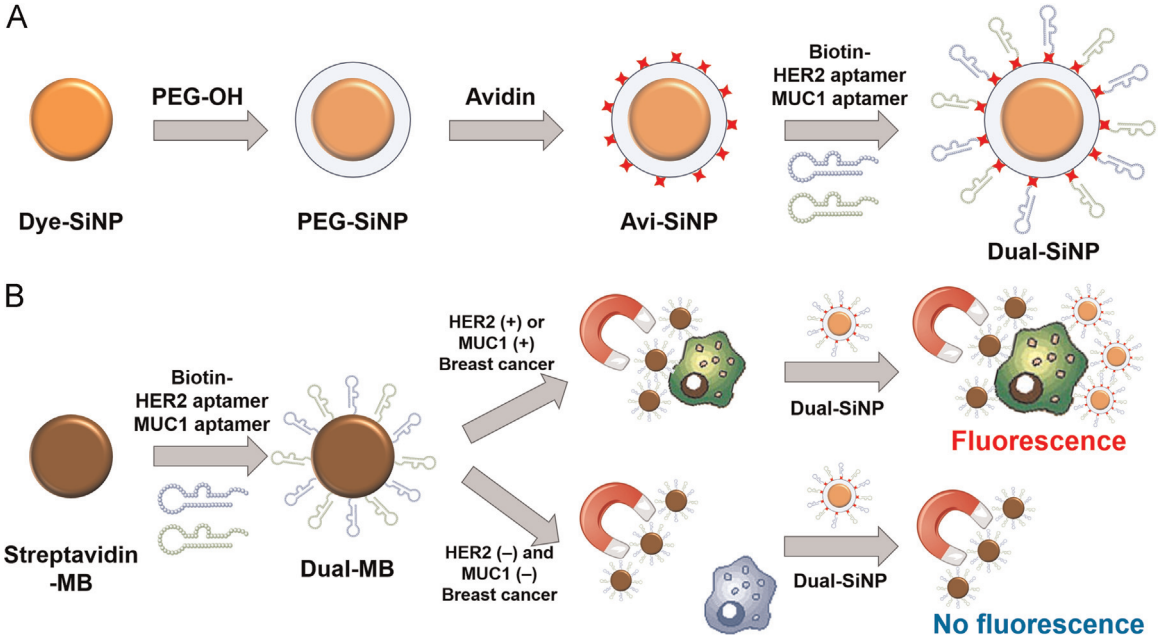

Fig. 1. (A) Modification processes of the silica nanoparticles. First, Dye-SiNPs were synthesized via the reverse microemulsion technique, and then, they were coated with PEG. Through CNBr activation, avidin was immobilized onto the PEG-SiNPs, and MUC1 and HER2 aptamers were functionalized by biotin-avidin interactions. (B) Schematic illustration of the selective detection for only MUC1(+) and HER2(+) breast cancer cells by Dual-SiNPs. MUC1(+) or HER2(+) breast cancer cells were selectively separated using dual aptamer-modified magnetic beads (Dual-MBs), and then, they were detected with Dual-SiNPs.

for 24 h at 4 °C. Then, 200 μL of 2% bovine serum albumin (BSA) in PBS was added to the solution, and the reaction was further maintained for 24 h at 4 °C. Avidin-modified PEG-SiNPs (Avi-SiNPs) were centrifuged, washed with PBS twice, and resuspended in PBS. To synchronously target both types of biomarkers, MUC1 and HER2, on the breast cancer cells, two aptamers were conjugated to Avi-SiNPs through avidin–biotin affinity. 5′-biotin-modified MUC1 aptamer (5′-biotin-GGGAGACAAGAA-TAAACGCTCAAGCAGTTGATCCTTTGGATACCCTGGTTCGA-CAGGAGGCTCACAACAGGC) and HER2 aptamer (5′-biotin-AACCGCCCAAATCCCTAAGAGTCTGCACTTGTCATTTTGTA-TATGTATTTGGTTTTTGGCTCTCACAGACACACTACACACGCACA) were purchased from Cosmo Genetech (Korea). These aptamers were utilized without further purification. Then, MUC1 and HER2 DNA aptamers in various ratios were incubated with 0.5 mg of Avi-SiNPs in PBS for 2 h at RT. Dual-SiNPs were centrifugally washed with PBS twice to remove unbound aptamers, resuspended in PBS, and stored at 4 °C.

2.2. Optimization of the aptamer ratio between MUC1 and HER2

Dual-SiNPs were prepared with the following three different ratios of the MUC1 aptamer to the HER2 aptamer: 1:1, 2:1, and 1:2. In addition to these, three different modifications of SiNPs with MUC1 aptamer, HER2 aptamer, and the control DNA were prepared and they were tested to confirm the binding affinity of Dual-SiNPs. 5′-biotin-modified control DNA (5′-biotin-AAAAAAAAAAAAAAACGTGCAGTACGCCAACCTTTCT-CATGCGCTGCCCCTCTTA) was purchased from Bionics (Korea). To minimize the disparity of the binding affinities between the two aptamers, each silica nanoparticle was treated to two types of cancer cell lines, including MCF-7 (MUC1 over-expressed breast cancer cells) and SK-BR-3 (HER2 over-expressed breast cancer cells). Each cell line was cultured in RPMI-1640 supplemented with 10% (v/v) fetal bovine serum (FBS), 100 U/mL penicillin G, and 100 mg/mL streptomycin at 37 °C in a 5% (v/v) CO_2 humid incubator. After the cells were cultured on a circular 100 π dish, they were trypsinized and resuspended in serum-free RPMI-1640 media. Fifty microliters of 5×10^4 cells were sub-cultured to 80% (v/v) occupation on a 60 mm × 15 mm culture dish in the humid CO_2 incubator. Prior to the treatment of the particles, they were washed three times with Dulbecco's Phosphate Buffered Saline (DPBS). Then, three types of particles with a concentration of 0.1 mg/mL were treated to both cell lines for 1 h at RT. Unbound particles were eliminated, and the treated cells were washed with DPBS three times. Finally, each cell was collected by a cell scraper, and the fluorescence spectra of the bound particles were obtained via a QuantaMaster (Photon Technology International, New Jersey, USA).

2.3. Binding test of the dual-SiNPs

To validate the binding affinity of the Dual-SiNPs, four breast cancer cell lines (MCF-7, T47D, SK-BR-3, and BT-474) were cultured on a 12 mm π cover glass consistent with the previously described conditions. After the cell confluency reached approximately 80% (v/v), each well was washed three times with DPBS and then fixed with a fixation solution (2% paraformaldehyde, 2% glutaraldehyde, and 0.05 M sodium cacodylate, pH 7.2) for 10 min at 4 °C. Additionally, the cells were blocked with 10 mg/mL BSA for 30 min at RT and washed with DPBS three times. The fixed cells were treated with 0.1 mg/mL Dual-SiNPs modified with the two aptamers in a ratio of 1:1 for 1 h at RT, followed by the removal of the unbound Dual-SiNPs and washing with DPBS three times. Fluorescent microscopic images of the cells were recorded using a Zeiss Axioplan 2 microscope with 20× objective (ZEISS, Germany). For the excitation of the SiNPs, a 455/70 nm band-pass filter was used when the images were recorded with a 515 nm long-pass filter to visualize the fluorescence signal from the bound particles. The resulting images were taken using a Zeiss Axiocam HR camera (ZEISS, Germany).

2.4. Quantitative detection of the breast cancer cells using silica nanoparticles

First of all, dual aptamer-modified magnetic particles (Dual-MBs) were prepared to selectively separate only breast cancer cells. Ten milligrams of streptavidin-modified magnetic particles were washed with a coupling buffer (5 mM Tris–HCl, pH 7.5, 1 M NaCl, 0.5 mM ethylenediaminetetraacetic acid tetrasodium, and 0.0025% (v/v) TWEEN-20) two times and incubated with 1 nmole of biotin-modified MUC1 and HER2 aptamers in the coupling buffer for 1 h at RT. After washing with the coupling buffer three times, the resulting particles were resuspended in PBS. Four types of cell lines (MCF-7, T47D, SK-BR-3, and BT-474) were cultured on the 100 π dish in accordance with the previously described conditions, and then they were detached with enzyme-free cell dissociation buffer to prevent damage to the surface proteins of the cells. The suspensions of each cell in the tube were combined with an equal volume of 0.1% (v/v) trypan blue solution for 5 min. Cells were placed in a hemocytometer, which counted the dead and viable cells, and then the viability of each cell was ensured. To construct the calibration curve, various concentrations of each cell were incubated with 0.1 mg of Dual-MBs in 100 μL of RPMI-1640 supplemented with 10% (v/v) FBS for 1 h at RT, and then the resulting particles were washed with PBS three times. Each particle–cell complex was left to react with 0.1 mg/mL of Dual-SiNPs for 1 h at RT. The unbound SiNPs were eliminated through PBS washing. The fluorescence intensities of each type of magnetic bead-cell-SiNP complex were measured via a Synergy HT Multi-Mode Microplate Reader (BioTeK, USA). The excitation and emission filters used were a 485/20 nm band-pass filter and a 590/35 nm band-pass filter, respectively. Based on the fluorescence intensities, the calibration curves of each cell were obtained using OriginPro 8.0 software (OriginLab). For the confirmation of the applicability of this system to real samples, human serum that was diluted 10 times with PBS was supplemented to reaction mixtures. Using only MCF-7 and SK-BR-3 cells, the detection was carried out as described above. And then, the calibration curves were constructed.

2.5. Selectivity test of the dual-SiNPs

The selectivity of the Dual-SiNPs was verified using MUC1(−) and HER2(−) cell lines, HepG2 (hepatocellular carcinoma) and CT26 (colon carcinoma). Four types of cell lines (MCF-7, SK-BR-3, HepG2, and CT26) were prepared as floating cells according to the previous method, and the viabilities and exact concentrations of them were determined by utilizing a hemocytometer. Several combinations of each cell were applied to the detection system, followed by analysis based on the microplate reader.

3. Results and discussion

3.1. Design of breast cancer-specific fluorescent silica nanoparticles

Since the development of the Stöber method for the synthesis of SiNPs, it has been widely utilized because it is simple, convenient, and time saving (Stöber et al., 1968). However, there are some drawbacks such as the heterogeneous sizes of the particles and the relatively low yield due to purification steps, resulting in

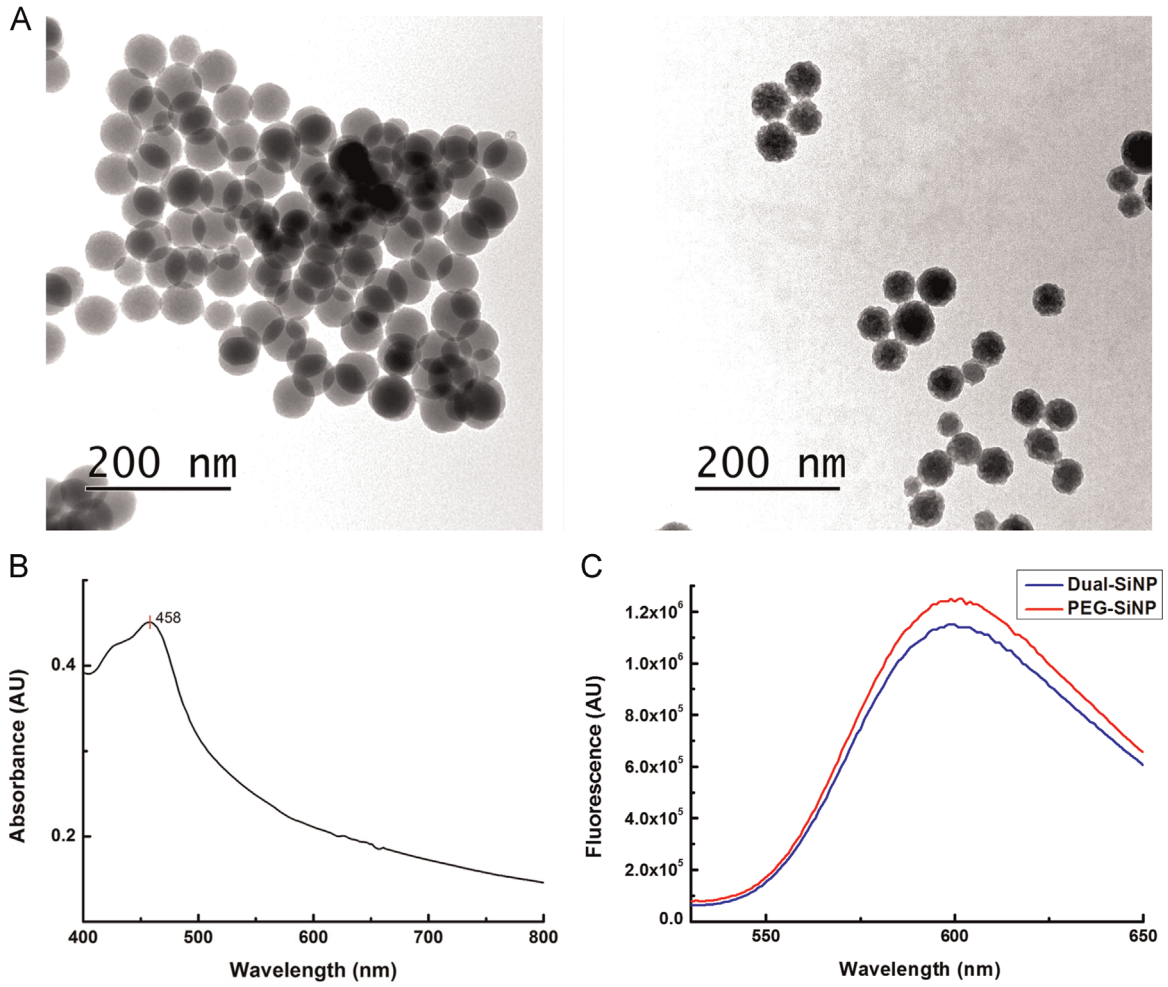

Fig. 2. The characterization of each type of SiNP. (A) The TEM images of PEG-SiNPs (left) and Dual-SiNPs (right). (B) The UV–vis absorbance spectrum of Dual-SiNPs. (C) The emission spectra of the two types of SiNPs, PEG-SiNPs and Dual-SiNPs (λ_{exi}= 458 nm).

demands for an alternative method. Recently, the synthesis of silica particles in nonionic water-in-oil microemulsions was developed, which provides a moderate consistency in the size and composition of the particles. Hence, the reverse microemulsion method was employed to prepare the detection probes. In addition, aptamers were introduced into this work as targeting molecules, which have attracted great attention as valuable biological ligands on account of their high sensitivity and selectivity (Famulok and Mayer, 2014; Kanwar et al., 2014; Song et al., 2012; Wang and Farokhzad, 2014). Aptamers are peptide or oligonucleic acid molecules that are small in size and have a good stability in severe conditions, such as in high temperatures and at low pH values. They have various benefits over antibodies, such as their easy modification, high stability, and economical production. Their convergence permits them to achieve ultra-sensitive detection of the target molecules.

The dual aptamer-modified SiNPs were prepared as described in supplementary data. As shown in Fig. 2A, PEG-SiNPs (left) were relatively homogeneous in their shapes and sizes, with an average diameter of 70 nm, whereas Dual-SiNPs (right) exhibited a bumpy surfaces, indicating that the shells of the particles were properly coated with aptamers. The functionalization of SiNPs was also validated through DLS, which provided information that the average sizes of the PEG-SiNPs and Dual-SiNPs were 78.74 ± 0.98 nm and 89.34 ± 2.01 nm, respectively. A consecutive increase in the sizes of the SiNPs revealed the successful modification of the surface. Moreover, the ξ-potentials of the particles were measured to quantify their surface charges. The ξ-potentials were -4.94 ± 0.27 mV (PEG-SiNPs) and -28.13 ± 5.00 mV (Dual-SiNPs). The high negative charge of DNA that arises from the phosphate groups, resulted in the ξ-potential of the Dual-SiNPs being more negative than that of the PEG-SiNPs. All of the physical traits of the newly synthesized particles substantiated the completion of the functionalization.

Not only morphological features but also spectroscopic characteristics of the silica nanoparticles were confirmed. Fig. 2B shows the absorbance spectrum of Dual-SiNPs, which demonstrated a maximum absorbance peak at 458 nm. This value coincides with the previously reported value (Bagwe et al., 2004; Thepwiwatjit et al., 2014). In addition, the emission spectra of the particles were obtained using a fluorometer. As shown in Fig. 2C, both PEG-SiNPs and Dual-SiNPs emitted maximum fluorescent signals at 600 nm, indicating that the immobilization of the aptamers on the silica nanoparticles did not affect the spectroscopic characteristics of the dye-doped silica nanoparticles. As result, it is desirable that the designed probe is a valuable tool for use in the diagnosis of breast cancer because of its homogeneous composition and great fluorescence.

Additionally, the amount of each aptamer on the surface of SiNPs was determined via an indirect fluorescent method-based on Hoechst 33258 (Cai et al., 2011). Because it has been known that Hoechst 33258 is strongly bound to only double-stranded DNA (dsDNA), and not to other biomolecules such as single-stranded DNA, proteins, and RNA (Barooah et al., 2011),

quantitative detection of dsDNA is possible. Therefore, the aptamer density of Dual-SiNPs was measured using this method. As shown in Fig. S1, calibration curves of MUC1 aptamer and HER2 aptamer were constructed using each biotin-modified aptamer and each complementary DNA. Both graphs exhibit good linear relationships between the concentration of the aptamers and the fluorescent signals, with a high squares of the correlation coefficients over 0.98. The regression equations of MUC1 aptamer and HER2 aptamer are $F=547.9C+12{,}365.8$ and $F=130.9C+3407.3$, respectively. The translation of mass of SiNPs into the number was already performed by Pang group (Cai et al., 2013). One milligram of SiNPs (~60 nm) approximately corresponds to 6.8 pmole. When 0.50 nM of Dual-SiNPs were separately incubated with complementary DNA of MUC1 and HER2, the fluorescence signals were 26,893.2 (±893.3) and 6980.8 (±913.1), respectively, indicating that about 53 MUC1 aptamers and 54 HER2 aptamers are immobilized on the surface of one Dual-SiNP.

3.2. Maximization of the binding affinity of the dual-SiNPs

Even though aptamers possess a prominent binding affinity to a target molecule, the binding extent of each aptamer is not equivalent. In particular, when multiple targeting probes are utilized, the comparative proportion of each probe should be optimized to achieve extremely sensitive detection. It has been shown that the two aptamers used in this work have different dissociation constants (K_d) of 0.135 nM for MUC1 and 18.9 nM for HER2 (Ferreira et al., 2006; Liu et al., 2012). Because the K_d values were measured using recombinant target proteins and were evaluated from separate detection systems, such as surface plasmon resonance and the magnetic bead-based method, the binding affinities of the aptamers to real targets, especially the breast cancer cells in this work, may not correlate with the K_d values. For this reason, the binding affinities of each type of Dual-SiNP with various aptamer ratios were demonstrated.

As shown in Fig. S2, each individual aptamer-modified functionalized nanoparticles exhibited higher fluorescence intensity than Dual-SiNPs (Fig. 3A). In the case of control DNA-modified SiNPs, low fluorescence signals were obtained for both types of the MUC1(+) cells (MCF-7) and HER2(+) cells (SK-BR-3), implying that synthesized Dual-SiNPs are bound to only MUC1(+) and HER2(+) cells via specific interaction between aptamers and target proteins. Dual-SiNPs with three different ratios of the MUC1 aptamer to the HER2 aptamer (1:1, 2:1, and 1:2) were applied to the MCF-7 cells and SK-BR-3 cells. As represented in Fig. 3A, each particle exhibited distinct tendencies with respect to its fluorescence intensity. A comparison of the emission fluorescence at 600 nm made the disparity more obvious (Fig. 3B). In the case of Dual-SiNPs modified with MUC1 and HER2 at a ratio of 1:1, the fluorescence signal was appropriate for both types of cell lines. In particular, the fluorescence values of MCF-7 were relatively higher than those of SK-BR-3, which might be caused by the following two main factors: the disparity in the K_d values of each aptamer and the expression profile of the target proteins in each cell. Although the quantification of protein expression in the cell lines offers valuable information with respect to the design of the detection system, any further discussion of this is beyond the scope of this paper. According to the results, the ratio of MUC1 to HER2 was optimized as 1:1.

3.3. Verification of the cytotoxicity of the detection probe

For the application of the detection particles for *in vivo* diagnosis, the detection probe must not display cytotoxicity. It is already known that both the MUC1 and HER2 DNA aptamers do not function as antagonists that interrupt cell metabolism or induce cell death via the suppression of the operations of key molecules (Ferreira et al., 2006; Liu et al., 2012). Therefore, it can be deduced that the toxicity of synthesized particles originates from the core silica particles. To access the cytotoxicity of Dual-SiNPs, six breast cancer cell lines (MCF-7, T47D, SK-BR-3, BT-474, MDA-MB-231, and MDA-MB-453) were cultured in a 96-well plate until the cells reached 80% (v/v) confluency. All of the types of cell lines showed high viability after treatment with the particles, implying that the cell viability did not depend on the concentration of the Dual-SiNPs and time (Fig. S3). In fact, the cytotoxicity of the probe does not directly influence the results in this work because the fluorescence signal is only proportional to the number of the target cells. Nevertheless, this result is still significant and implies that the use of Dual-SiNPs is sufficiently applicable to *in vivo* diagnosis.

3.4. Microscopic analysis of the selective binding of dual-SiNPs

Before the quantification of the cells, the binding appearance of the Dual-SiNPs was analyzed using a Zeiss Axioplan 2 microscope. Each cell was fixed with the fixation solution, blocked with BSA, and then incubated with Dual-SiNPs. As displayed in Fig. 4, the red fluorescence of the Dual-SiNPs was quite uniformly distributed in the fluorescence figures. It seems that the partial particles are localized on the surfaces of the cells because the figures are two-dimensional images, regardless of depth. Nonetheless, the newly synthesized silica nanoparticles have high binding affinities to all of the cell lines that over-express MUC1 or HER2, including MCF-7, T47D, SK-BR-3, and BT-474. It is likely that Dual-SiNPs are readily

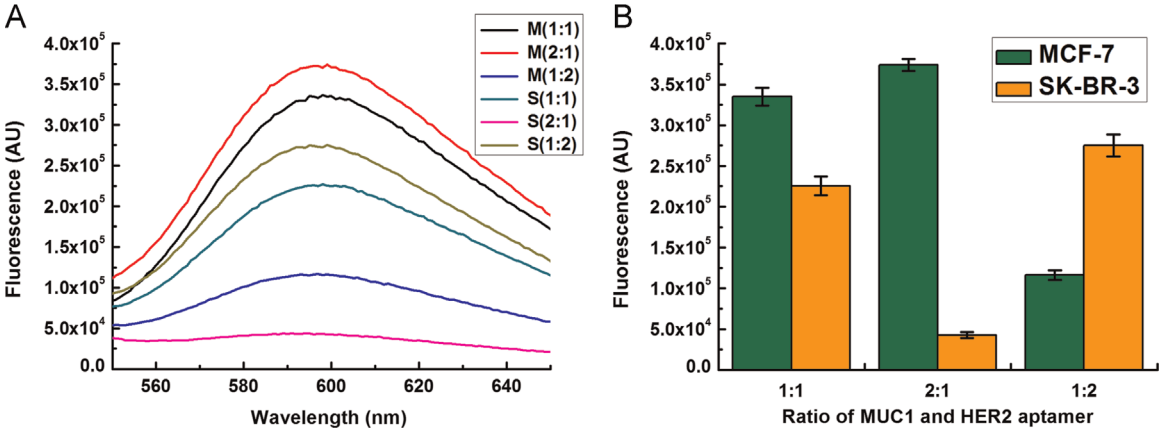

Fig. 3. Optimization of the ratio between the MUC1 and HER2 aptamers. (A) The emission spectra of the Dual-SiNPs with three different ratios of the MUC1 aptamer to the HER2 aptamer (1:1, 2:1, and 1:2). (M: MCF-7; S: SK-BR-3) (B) The fluorescent emission signal at 600 nm in each emission spectrum.

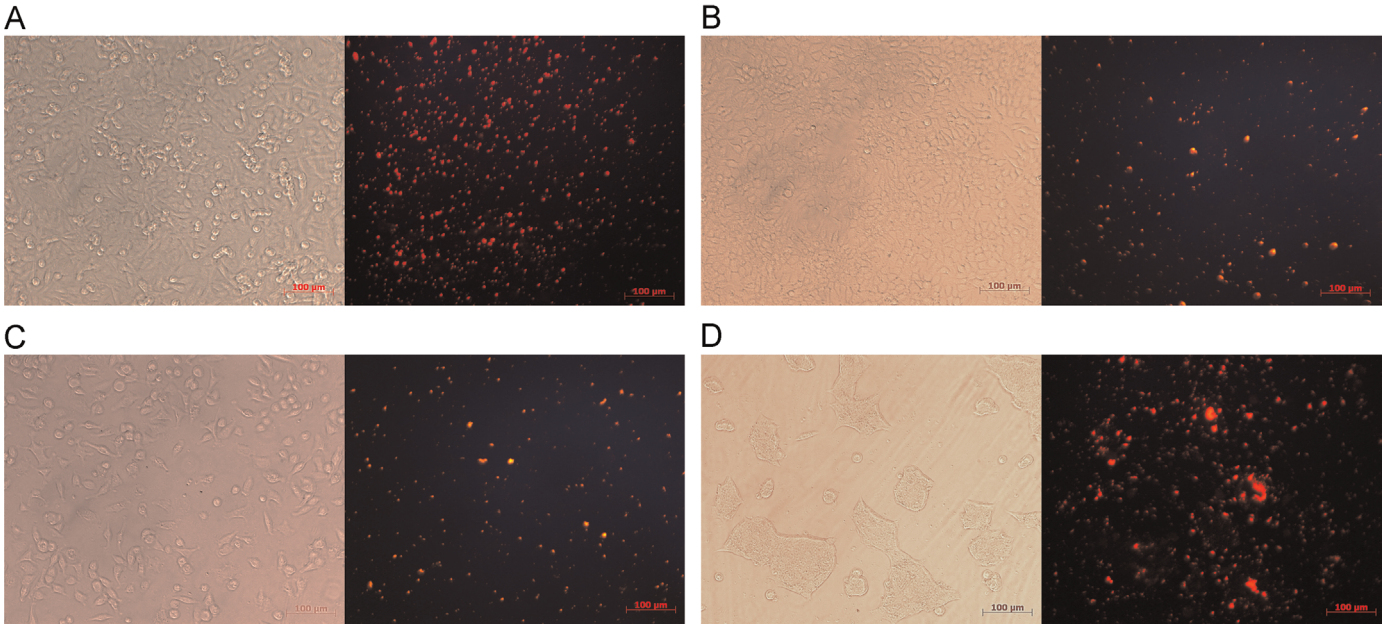

Fig. 4. The binding aspects of Dual-SiNPs to four types of breast cancer cell lines. Each cell was incubated with 0.1 mg/mL Dual-SiNPs for 1 h. Fluorescent microscopic images of the cells were recorded using a Zeiss Axioplan 2 microscope with a 20 × objective. (A) MCF-7, (B) T47D, (C) SK-BR-3 and (D) BT-474.

applicable for the diagnosis of breast cancer with a high affinity and selectivity.

3.5. Fabrication of a detection platform for breast cancer

After CTCs from breast cancer patients were determined to be beneficial markers for the diagnosis of breast cancer, they have received attention from numerous researchers. Various studies on the detection and prognosis of breast cancer have been conducted (Krawczyk et al., 2013; Lopez-Munoz and Mendez-Montes, 2013; Lu et al., 2010). However, most investigations, including CELLSEARCH®, are based on antibodies to the surface biomarkers of the cancer cells (Cristofanilli et al., 2004; Jiang et al., 2013). The deficiency of biomarkers for breast cancer makes the CTC detection of breast cancer restrictive. The introduction of dual aptamers can help to resolve these difficulties. The aptamer-based detection platform is more stable and cheaper than the antibody-based system, and the combination of MUC1 and HER2 enables a broad detection range for breast cancer. Dual aptamer-modified probe enables multi-targeting of samples in contrast with single aptamer-modified probe. Additionally, whereas various fluorescent dyes, such as cyanine3 (Cy3), Cy5, and fluorescein isothiocyanate (FITC), tend to suffer from photobleaching in biological conditions, the doped $Ru(BPY)_3$ molecule inside the silica nanoparticle has high a resistance toward photobleaching through electrostatic interactions (Cai et al., 2013). As represented in Fig. 1, the quantification of the cells progresses through the following two steps: separation and detection. Initially, MUC1(+) and HER2(+) cells are selectively separated from the cell mixture using Dual-MBs, and then, the Dual-MB–cell complexes are incubated with Dual-SiNPs. The fluorescence of the resulting complexes is obtained is proportional to the cell number, leading to quantification of the cells.

Four cell lines, including MCF-7, T47D, SK-BR-3, and BT-474, were utilized to confirm the sensitivity of the detection system. Calibration curves for each cell line were constructed as shown in Fig. 5. All of the graphs exhibit good linear relationships between the concentration of the cells and the fluorescence emitted from the Dual-SiNPs, with a high squares of the correlation coefficients over 0.98. The detection was performed up to a cell concentration

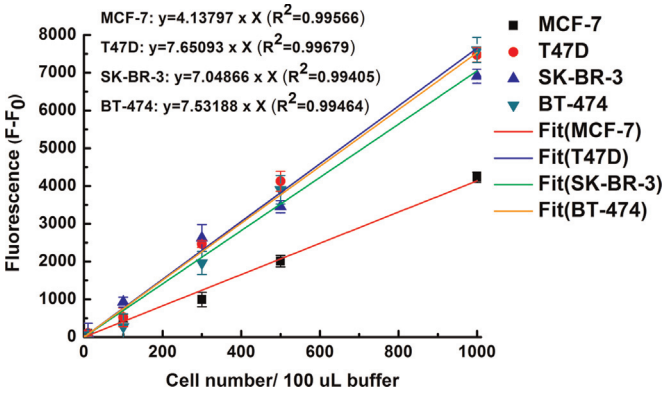

Fig. 5. The calibration curves for each breast cancer cell line (MCF-7, T47D, SK-BR-3, and BT-474). All of the curves were plotted using OriginPro 8.0 software (OriginLab).

of 1 cell/100 μL because systematic errors from the use of the hemocytometer and sequential dilution of the cells were inevitable, resulting in the detection of a concentration of cells under 1 cell/100 μL being meaningless. In other investigations, remarkable detection limits have been accomplished, such as chip-based detection (10 cells/mL), enzyme-linked immunosorbent assay (ELISA)-based detection (1 cell/mL), size selective microcavity array (1 cell/mL), and the PCR-based method (0.75 cell/mL) (Alix-Panabieres et al., 2009; Hosokawa et al., 2010; Iakovlev et al., 2008; Nagrath et al., 2007; Stott et al., 2010). A direct comparison of the detection limits is not significant because the methods for the calculation of the detection limits do not coincide. If the reaction volume is increased up to 1 mL and the cell number is counted more accurately, the detection limit of our system could be improved. It is anticipated that this detection platform could be a convenient diagnostic tool for breast cancer.

Furthermore, the applicability of this detection system to real samples was confirmed using human serum. Human serum was added to reaction mixtures, and then the detection was performed according to the same procedure as described above. As represented in Fig. S4, the calibration graphs of MCF-7 and SK-BR-3 exhibit fairly good linear relationships between the concentration

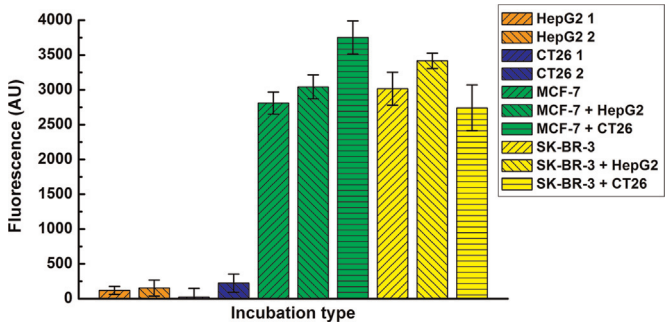

Fig. 6. Verification of the selectivity of the Dual-SiNPs. (HepG2 1: 500 cells of HepG2; HepG2 2: 1000 cells of HepG2; CT26 1: 500 cells of CT26; CT26 2: 1000 cells of CT26; MCF-7: 500 cells of MCF-7; MCF-7+HepG2: 500 cells of MCF-7+500 cells of HepG2; MCF-7+CT26: 500 cells of MCF-7+500 cells of CT26; SK-BR-3: 500 cells of SK-BR-3; SK-BR-3+HepG2: 500 cells of SK-BR-3+500 cells of HepG2; SK-BR-3+CT26: 500 cells of SK-BR-3+500 cells of CT26).

of the cells and the fluorescence, with a high squares of the correlation coefficients over 0.9, which is lower than those of graphs in Fig. 5. Although the detection limit was decreased as 10 cells/100 μL, this result suggests that the proposed detection platform is sufficiently applicable to real samples.

3.6. *Confirmation of the selectivity of the detection system*

It is imperative that the proposed biosensor exhibits a high selectivity to only breast cancer for a precise diagnosis. Therefore, the specificity of the sensing platform was evaluated using other cancer cell lines to validate the applicability of this system. It is widely known that both HepG2 (the hepatocellular carcinoma cell line) and CT26 (the colon carcinoma cell line) do not over-express MUC1 and HER2. These cells as well as MCF-7 and SK-BR-3 were applied to the detection system, and then, the resulting signals were recorded according to the previous experiment (Fig. 6). In the case of the MUC1(−) and HER2(−) cell lines, an increase in the cell number did not influence the signal changes in the fluorescence (first column to fourth column). By contrast, a high fluorescence was obtained for the MUC1(+) and HER2(+) cell lines (fifth column and eighth column). The addition of MUC1(−) and HER2(−) cell lines to MCF-7 or SK-BR-3 did not cause a remarkable variation in the fluorescence values. This result shows that the newly designed detection tool based on dual aptamer-modified silica nanoparticles can be a powerful platform for diagnosing a wide range of breast cancer.

4. Conclusions

Most of the studies that relate to breast cancer-specific detection are restricted within narrow limits because of the deficiency of promising markers. Based on the fact that HER2 and MUC1 are over-expressed in breast cancer cell lines, we designed novel diagnostic complexes, dual aptamer-modified silica nanoparticles (dye-doped), for the simultaneous targeting of breast cancers including HER2(+) and MUC1(+) cells. Unlike single aptamer-modified probe, this probe offers effective detection of breast cancer cells. The newly synthesized probe was characterized by various methods, such as transmission electron microscopy, dynamic light scattering, zeta potential measurement, ultraviolet–visible spectroscopy, and fluorescence spectroscopy. The dye-doped silica nanoparticles exhibited homogeneity in size, a negative surface charge, and a robust fluorescent signal. Furthermore, the developed particles were subjected to a cytotoxicity test, binding test, and selectivity confirmation, with the results indicating that the non-toxic probes were highly sensitive and selective to HER2(+) and MUC1(+) breast cancer cells. Although this aptamer-based detection system is the first system to target MUC1(+) and HER2(+) breast cancer cells synchronously with a high sensitivity and selectivity, our work is limited to *in vitro* diagnosis only. To apply this probe to *in vivo* systems, several difficulties need to be overcome, such as the instability of nucleic acids in the blood, the short half-life of the silica nanoparticles in circulation, and the degradation of the fluorescence signal of the probe in the blood. If further attempts and investigations are performed, it is anticipated that the dual aptamer-modified silica nanoparticles will be a promising diagnostic nanomaterial for breast cancer as well as for other types of cancer.

Acknowledgements

This work was supported by the National Research Foundation of Korea (NRF- 2014029297) and a grant of the Korea Health Technology R&D Project through the Korea Health Industry Development Institute (KHIDI), funded by the Ministry of Health and Welfare, Republic of Korea (Grant no.: HI12C-1852-020013).

Appendix A. Supplementary information

Supplementary data associated with this article can be found in the online version at http://dx.doi.org/10.1016/j.bios.2015.04.030.

References

Alama, A., Truini, A., Coco, S., Genova, C., Grossi, F., 2014. Drug Discov. Today 19, 1671–1676.
Alix-Panabieres, C., Vendrell, J.P., Slijper, M., Pelle, O., Barbotte, E., Mercier, G., Jacot, W., Fabbro, M., Pantel, K., 2009. Breast Cancer Res., 11.
Bagwe, R.P., Yang, C., Hilliard, L.R., Tan, W., 2004. Langmuir 20, 8336–8342.
Barooah, N., Mohanty, J., Pal, H., Sarkar, S.K., Mukherjee, T., Bhasikuttan, A.C., 2011. Photochem. Photobiol. Sci. 10, 35–41.
Bertolini, F., Shaked, Y., Mancuso, P., Kerbel, R.S., 2006. Nat. Rev. Cancer 6, 833–845.
Bidard, F.C., Fehm, T., Ignatiadis, M., Smerage, J.B., Alix-Panabieres, C., Janni, W., Messina, C., Paoletti, C., Muller, V., Hayes, D.F., Piccart, M., Pierga, J.Y., 2013. Cancer Metastasis Rev. 32, 179–188.
Cai, L., Chen, Z.Z., Dong, X.M., Tang, H.W., Pang, D.W., 2011. Biosens. Bioelectron. 29, 46–52.
Cai, L., Chen, Z.Z., Chen, M.Y., Tang, H.W., Pang, D.W., 2013. Biomaterials 34, 371–381.
Chang, K., Pi, Y., Lu, W., Wang, F., Pan, F., Li, F., Jia, S., Shi, J., Deng, S., Chen, M., 2014. Biosens. Bioelectron. 60, 318–324.
Cristofanilli, M., Budd, G.T., Ellis, M.J., Stopeck, A., Matera, J., Miller, M.C., Reuben, J. M., Doyle, G.V., Allard, W.J., Terstappen, L.W., Hayes, D.F., 2004. N. Engl. J. Med. 351, 781–791.
Famulok, M., Mayer, G., 2014. Chem. Biol. 21, 1055–1058.
Ferreira, C.S.M., Matthews, C.S., Missailidis, S., 2006. Tumor Biol. 27, 289–301.
Gazzaniga, P., Gianni, W., Raimondi, C., Gradilone, A., Lo Russo, G., Longo, F., Gandini, O., Tomao, S., Frati, L., 2013. Tumor Biol. 34, 2507–2509.
Gupta, G.P., Massague, J., 2006. Cell 127, 679–695.
Gupta, S., Thirstrup, D., Jarvis, T.C., Schneider, D.J., Wilcox, S.K., Carter, J., Zhang, C., Gelinas, A., Weiss, A., Janjic, N., Baird, G.S., 2011. Appl. Immunohistochem. Mol. Morphol. 19, 273–278.
Herr, J.K., Smith, J.E., Medley, C.D., Shangguan, D., Tan, W., 2006. Anal. Chem. 78, 2918–2924.
Hosokawa, M., Hayata, T., Fukuda, Y., Arakaki, A., Yoshino, T., Tanaka, T., Matsunaga, T., 2010. Anal. Chem. 82, 6629–6635.
Howes, P.D., Chandrawati, R., Stevens, M.M., 2014. Science 346, 1247390.
Iakovlev, V.V., Goswami, R.S., Vecchiarelli, J., Arneson, N.C.R., Done, S.J., 2008. Breast Cancer Res. Treat. 107, 145–154.
Jeon, W., Lee, S., Manjunatha, D.H., Ban, C., 2013. Anal. Biochem. 439, 11–16.
Jiang, Z.F., Cristofanilli, M., Shao, Z.M., Tong, Z.S., Song, E.W., Wang, X.J., Liao, N., Hu, X.C., Liu, Y., Wang, Y., Zeng, L., Zhang, M., 2013. Ann. Oncol. 24, 2766–2772.
Johnson, R.H., Chien, F.L., Bleyer, A., 2013. JAMA, J. Am. Med. Assoc. 309, 800–805.
Kanwar, J.R., Shankaranarayanan, J.S., Gurudevan, S., Kanwar, R.K., 2014. Drug Discov. Today 19, 1309–1321.
Krawczyk, N., Banys, M., Hartkopf, A., Hagenbeck, C., Melcher, C., Fehm, T., 2013. Ecancermedicalscience 7, 352.
Lee, S., Manjunatha, D.H., Jeon, W., Ban, C., 2014. PLoS ONE, 9.

Li, H., Mu, Y., Lu, J., Wei, W., Wan, Y., Liu, S., 2014. Anal. Chem. 86, 3602–3609.
Liu, J.S., Zang, L.J., Wang, Y.R., Liu, G.N., 2014. J. Lumin. 147, 155–158.
Liu, Z., Duan, J.H., Song, Y.M., Ma, J., Wang, F.D., Lu, X., Yang, X.D., 2012. J. Transl. Med., 10.
Lopez-Munoz, E., Mendez-Montes, M., 2013. Adv. Clin. Chem. 61, 175–224.
Lu, W., Arumugam, S.R., Senapati, D., Singh, A.K., Arbneshi, T., Khan, S.A., Yu, H., Ray, P.C., 2010. ACS Nano 4, 1739–1749.
March, S.C., Parikh, I., Cuatrecasas, P., 1974. Anal. Biochem. 60, 149–152.
Mostert, B., Sleijfer, S., Foekens, J.A., Gratama, J.W., 2009. Cancer Treat. Rev. 35, 463–474.
Nadal, R., Lorente, J.A., Rosell, R., Serrano, M.J., 2013. Expert Rev. Mol. Diagn. 13, 295–307.
Nagrath, S., Sequist, L.V., Maheswaran, S., Bell, D.W., Irimia, D., Ulkus, L., Smith, M.R., Kwak, E.L., Digumarthy, S., Muzikansky, A., Ryan, P., Balis, U.J., Tompkins, R.G., Haber, D.A., Toner, M., 2007. Nature 450, 1235–1239.
Pantel, K., Alix-Panabieres, C., 2010. Trends Mol. Med. 16, 398–406.
Pantel, K., Brakenhoff, R.H., Brandt, B., 2008. Nat. Rev. Cancer 8, 329–340.
Pukazhendhi, G., Gluck, S., 2014. J. Carcinog. 13, 8.
Rakha, E.A., Boyce, R.W., Abd El-Rehim, D., Kurien, T., Green, A.R., Paish, E.C., Robertson, J.F., Ellis, I.O., 2005. Mod. Pathol. 18, 1295–1304.
Siegel, R., Naishadham, D., Jemal, A., 2013. CA Cancer J. Clin. 63, 11–30.
Singh, J., Sharma, S., Nara, S., 2015. Food Chem. 170C, 470–483.
Singh, R., Bandyopadhyay, D., 2007. Cancer Biol. Ther. 6, 481–486.
Slamon, D.J., Clark, G.M., Wong, S.G., Levin, W.J., Ullrich, A., McGuire, W.L., 1987. Science 235, 177–182.
Smith, J.E., Medley, C.D., Tang, Z., Shangguan, D., Lofton, C., Tan, W., 2007. Anal. Chem. 79, 3075–3082.
Song, K.M., Lee, S., Ban, C., 2012. Sensors 12, 612–631.
Stöber, W., Fink, A., Bohn, E., 1968. J. Colloid Interface Sci. 26, 62–69.
Stott, S.L., Hsu, C.H., Tsukrov, D.I., Yu, M., Miyamoto, D.T., Waltman, B.A., Rothenberg, S.M., Shah, A.M., Smas, M.E., Korir, G.K., Floyd, F.P., Gilman, A.J., Lord, J.B., Winokur, D., Springer, S., Irimia, D., Nagrath, S., Sequist, L.V., Lee, R.J., Isselbacher, K.J., Maheswaran, S., Haber, D.A., Toner, M., 2010. Proc. Natl. Acad. Sci. USA 107, 18392–18397.
Thepwiwatjit, N., Thattiyaphong, A., Limsuwan, P., Tuitemwong, K., Tuitemwong, P., 2014. J. Nanomater., 2014.
Wang, A.Z., Farokhzad, O.C., 2014. J. Nucl. Med. 55, 353–356.
Wang, H.Y., Ahn, S., Kim, S., Park, S., Park, S., Han, H., Sohn, J.H., Kim, S., Lee, H., 2014. Exp. Mol. Pathol. 97, 445–452.
Wang, K., He, X., Yang, X., Shi, H., 2013. Acc. Chem. Res. 46, 1367–1376.
Zhao, S., Yang, H.K., Zhang, M.H., Zhang, D.K., Liu, Y.P., Liu, Y., Song, Y., Zhang, X.S., Li, H.B., Ma, W.J., Zhang, Q.Y., 2013. Cell Biochem. Biophys. 65, 263–273.
Zhu, Y., Chandra, P., Shim, Y.B., 2013. Anal. Chem. 85, 1058–1064.